A Coupled FDTD-Artificial Neural Network Technique for Large-Signal Analysis of Microwave Circuits

S. Goasguen, S. M. El-Ghazaly

Telecommunications Research Center, Department of Electrical Engineering, Arizona State University, Phoenix, Arizona 85287-5706

Received 11 March 2001; accepted 24 August 2001

ABSTRACT: We propose a first-order global modeling approach of Monolithic Microwave Integrated Circuits (MMIC) by modeling the active device with a neural network based on a full hydrodynamic model. This neural network describes the nonlinearities of the equivalent circuit parameters of an MESFET implemented in an extended Finite Difference Time Domain mesh to predict large-signal behaviors of the circuits. We successfully represented the transistor characteristics with a one-hidden-layer neural network, whose inputs are the gate voltage V_{gs} and the drain voltage V_{ds}. The trained neural network shows excellent accuracy and dramatically reduces the computational time in comparison with the hydrodynamic model. Small-signal simulation is performed and validated by comparison with HP-Libra. Then large-signal behaviors are obtained, which demonstrates the successful use of the artificial neural network. © 2002 John Wiley & Sons, Inc. Int J RF and Microwave CAE 12: 25–36, 2002.

Keywords: neural network; extended-FDTD; microwave circuits; global modeling

I. INTRODUCTION

Microwave circuits are more and more integrated. In the millimeter-wave (mm-wave) band, the radiation and the coupling effects cannot be neglected anymore. In most commercial microwave design software, simulations are performed according to the circuit theory approach. Therefore, the electromagnetic coupling between different circuit elements is ignored. However, an accurate mm-wave design is possible, but the devices modeling process is extremely lengthy and costly. The "Global Modeling" technique tends to unify both the electromagnetic analysis of passive structures and the semiconductor theory used to obtain physical models of transistors. If this could be achieved, then the trial and error procedure used in conventional design would be avoided. Moreover, the performances of new transistors in a specific microwave circuit could be analyzed without any fabrication.

At very high frequencies, the active device model must be accurate enough to predict the behavior of submicrometer gate devices. Alsunaidi et al. [1] have used a full hydrodynamic model coupled with Maxwell's equations to predict the interactions between the carriers and the propagating wave inside the device. Recently, this full hydrodynamic model has been used to demonstrate the global modeling approach [2]. A complete amplifier has been simulated taking into account all electromagnetic effects, namely radiation, coupling, and wave-device interactions. However, a practical implementation of this tech-

Correspondence to: S. El-Ghazaly; e-mail: sme@asu.edu.
Contract grant sponsor: U.S. Army Research Office.
Contract grant number: DAAH04-95-1-0252.

DOI 10.1002/mmce.10018

nique is difficult. The mesh density in the device region is much smaller than the one in the passive structures. Therefore, time-consuming techniques such as nonuniform meshing and time domain diakoptics [3], must be employed to solve this problem.

Artificial neural network (ANN) is a new trend in mm-wave CAD that dramatically reduces the computation time of electromagnetic (EM) models and replaces the expensive EM model with ANN trained by EM simulation results [4]. This new approach has been successfully used [5–7] to model passive devices, such as CPW structures, spiral inductors, and interconnects. In [8, 9], neural networks are used to design a microstrip corporate feed and also to optimize interconnects in high-speed VLSI circuits. ANNs have also been used to model the high nonlinearities of transistors obtained by measurements or empirical models [10, 11]

The extended FDTD approach suggests to include nonlinear devices in the FDTD grid as in [12–14]. This method leads to an equivalent circuit that characterizes the wave-device interactions, which gives a good approximation of a global modeling simulation providing that the transistor model comes from a semiconductor simulation.

In this article, we propose to model the steady-state solution of the hydrodynamic equations by an artificial neural network that accurately and efficiently predicts the behavior of the simulated MESFET. The transistor is implemented in an extended FDTD code to simulate an amplifier. The nonlinearities of the MESFET are described by the ANN, which updates the circuit parameters values inside the FDTD mesh according to the electromagnetic field computed. This new approach provides a very efficient and practical first-order global modeling of an MMIC.

The article is organized as follows. Section 2 begins with a review of the hydrodynamic model. Section 3 describes artificial neural network and gives a very comprehensive matrix formulation. In Section 4, the extended FDTD approach is reviewed, the simulated structure is presented, and the interaction with the ANN is explained. Section 5 presents the results of the ANN model compared with the hydrodynamic model. To validate the method, the frequency response of the small-signal simulation is compared with HP-Libra. The time domain responses of the small signal and large-signal simulations are also shown. Finally, conclusions are drawn in Section 6.

II. HYDRODYNAMIC MODEL

This model is based on the moments of the Boltzmann transport equations obtained by integration over the momentum space [1]. These equations provide a time-dependent solution for carrier density, energy, and momentum. They are given below:

Current continuity

$$\frac{\partial n}{\partial t} + \nabla \cdot (nv) = 0.$$

Energy conservation

$$\frac{\partial (n\varepsilon)}{\partial t} + \nabla \cdot (nv\varepsilon) = qnv \cdot E - \nabla v \cdot (nkTv) - \frac{n(\varepsilon - \varepsilon_0)}{\tau_\varepsilon}.$$

Momentum conservation

$$\frac{\partial (np_x)}{\partial t} + \nabla \cdot (np_x v) = qnE_x - \nabla(nkT) - \frac{np_x}{\tau_m},$$

where n is the carrier density, v is the carrier velocity, p is the carrier momentum, k is the Boltzmann constant, and T is the temperature. The energy and momentum relaxation time are τ_ε and τ_m, respectively, E is the electric field, and ε is the energy. The time and spatial dependencies are not neglected to appropriately model submicrometer gate devices. The variations in effective mass with respect to time, space, and electron energy are also included in our work. This semiconductor device model is coupled with Maxwell's equations:

$$\nabla \times E = -\mu \frac{\partial H}{\partial t},$$

$$\nabla \times H = \varepsilon \frac{\partial E}{\partial t} + J,$$

where ε represents the dielectric constant and not the energy like in the previous equations. $\boldsymbol{J}$ represents the current density inside the device:

$$J(t) = -qn(t)v(t).$$

The simulation starts by obtaining the steady-state dc solution. Then this solution is used as initial values to solve Maxwell's equations on ac excitation. The curl of H and the electric field can then be defined as in [1]. Hence, a full-wave

analysis is performed inside the device to model traveling wave effects and wave-device interactions. Those equations are coupled highly nonlinear partial differential equations. An explicit finite difference scheme is used to decouple these equations. The solution is computed on a nonuniform orthogonal grid to improve accuracy and convergence speed. A fine grid is used in the regions, such as under the gate and in the active layer region, where high carrier-density gradients are observed. A coarse grid is used in neutral regions far from the depletion region. Stability of the algorithm is obtained by carefully choosing the finite difference scheme. The scheme must preserve the properties of the continuous partial difference equation: conservative and transportive.

This model has been successfully used to obtain a full-wave analysis of the transistor. However, this approach is computationally very expensive, and it is unpractical to perform design optimizations, as well as yield analysis. The training property of the ANN is used to speed up the full-wave analysis to efficiently characterize the large-signal behaviors of microwave circuits.

III. ARTIFICIAL NEURAL NETWORK

Figure 1 shows a three-layer neural network. There are two inputs, viz. gate-to-source voltage V_{gs} and drain-to-source voltage V_{ds}, and five outputs, viz. the drain current I_{ds}, the gate-to-drain capacitance C_{gd}, the drain-to-source capacitance C_{ds}, the gate-to-source capacitance C_{ds}, and the drain-to-source resistance R_{ds}.

The input of each neuron in the hidden layer is the sum of all the outputs of the input layer multiplied by a set of weighting factors. The output is given by a so-called activation function, which is a nonlinear function applied to the input to correctly model our data. The adaptability of the network is defined as the discrepancy between the outputs given by the network and the desired outputs. The computation of the outputs can be seen as a simple multiplication of matrices.

Let us consider a general three-layer neural network, with l input, m hidden neurons, and n outputs. Let X_{in} be a set of input values, the weighting factors can be stored in a matrix W_{in}.

$$X_{in} = \begin{bmatrix} x_1^{in} \\ x_2^{in} \\ \vdots \\ x_{l-1}^{in} \\ x_l^{in} \end{bmatrix}, \quad W_{in} = \begin{bmatrix} w_{1,1}^{in} & \cdots & w_{1,l}^{in} \\ \vdots & \ddots & \vdots \\ w_{m,1}^{in} & \cdots & w_{m,l}^{in} \end{bmatrix}$$

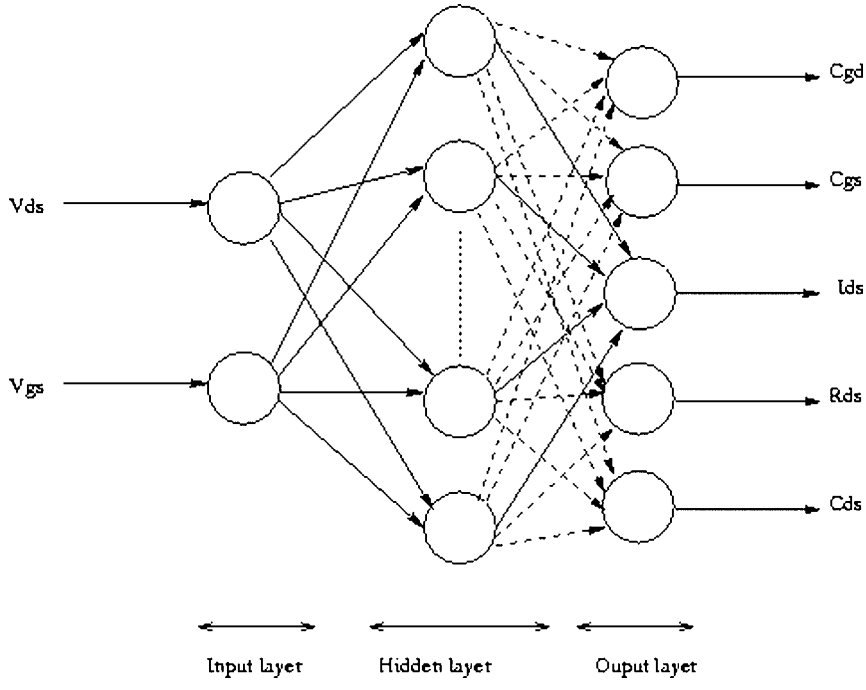

Figure 1. Three-layer artificial neural network.

Then the input of the hidden neurons is a vector I_{in} computed as the multiplication of X_{in} and W_{in}.

$$I_{\text{in}} = \begin{bmatrix} i_1 \\ \vdots \\ i_m \end{bmatrix} = W_{\text{in}} \cdot X_{\text{in}}.$$

The output of the hidden neurons is a vector I_{out} obtained by applying the activation function to the vector I_{in}. We chose to use a hyperbolic tangent function shown below.

$$I_{\text{out}} = \text{tsig}(I_{\text{in}}) \quad \text{with} \quad \text{tsig}(x) = \frac{2}{1+\exp(-2\cdot x)} - 1$$

Finally, the output of the neural network is obtained in the same way as the input of the hidden layer. One has to multiply the hidden layer output vector I_{out} and a weighting factor matrix W_{out}.

$$X_{\text{out}} = \begin{bmatrix} x_1^{\text{out}} \\ \vdots \\ x_n^{\text{out}} \end{bmatrix} \quad W_{\text{out}} = \begin{bmatrix} w_{1,1}^{\text{out}} & \cdots & w_{1,m}^{\text{out}} \\ \vdots & \ddots & \vdots \\ w_{n,1}^{\text{out}} & \cdots & w_{n,m}^{\text{out}} \end{bmatrix}$$

$$X_{\text{out}} = W_{\text{out}} \cdot I_{\text{out}}$$

This procedure computes the output of the neural network for a given input vector.

A set of data obtained from the steady-state solution of the hydrodynamic model is used to train the network and therefore optimize the weights. The data are normalized to speed up the convergence; and the *Levenberg–Marquardt* method is used to update the weighting factors. The number of neurons in the hidden layer is optimized to avoid over training and to give a good accuracy for testing data. Figure 2 presents the average error for different number of neurons in the hidden layer. It can be seen that for 6 neurons in the hidden layer, the RMS error is the same for training as for testing.

If much more neurons are needed to accurately model the nonlinearities, then a multilayer neural network can also be used [11] to reduce the number of neurons.

IV. COUPLED FDTD AND ANN APPROACH

Commercial design softwares are based on circuit approach. To perform a more accurate and efficient simulation of MMICs, the extended FDTD method employs equivalent current/voltage sources to substitute the device inside the FDTD grid [12]. Lumped elements such as resistor, capacitor and inductor can also be directly included in the FDTD marching time algo-

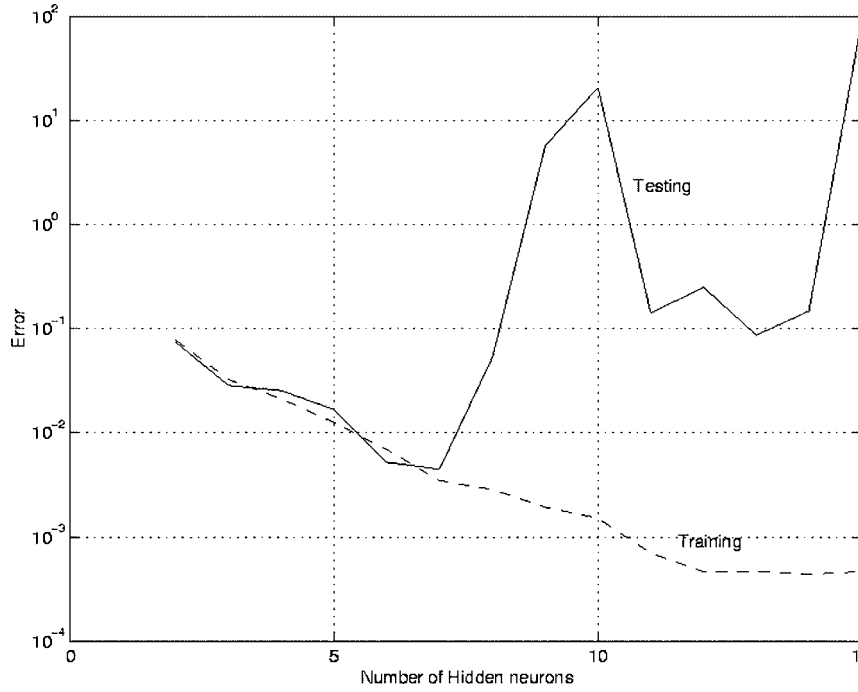

Figure 2. Error curves for training and testing data.

rithm [13, 14]. This technique has been used to simulate active antenna and amplifier [15, 16] and was connected to SPICE simulator to analyze more complicated transistor models or loads.

In this article we restricted ourselves to an intrinsic transistor model due to the results obtained from the hydrodynamic model and for simplicity of implementation in the FDTD mesh. Figure 3 shows the basic amplifier that is to be simulated using the extended FDTD approach. Parallel and series lumped elements can be inserted in a cell by adding the current density flowing through this cell, due to the presence of the lumped element. Single loads have been investigated [13, 14]. Here, we present the implementation of a parallel resistance and capacitance with a current source. This represents the drain-to-source resistance and drain-to-source capacitance plus the drain current source of the drain of a transistor. Each lumped element is distributed in each cell, hence the value of the actual lumped element per cell is not the total value of the lumped element. Figure 4 presents an insight into the meshing of the structure at the location of the transistor. This represents only a section of the actual structure and it repeats over the number of cells under the transmission line. If the lumped elements inserted are in the y direction, then the actual value of those parameters per cell is as follows:

$$R_{\text{cell}} = \frac{n_x}{n_y} R_{\text{total}} \quad \text{and} \quad C_{\text{cell}} = \frac{n_y}{n_x} C_{\text{total}},$$

where n_x and n_y are the number of cells below the microstrip in the x and y directions.

The general update formula of the electric field in the FDTD scheme is given by

$$E|_{i,j,k}^{n+1} = E|_{i,j,k}^{n} + \frac{\Delta t}{\varepsilon} * \nabla \times H|_{i,j,k}^{n+\frac{1}{2}} - \frac{\Delta t}{\varepsilon} * J_{\text{total}},$$

where $J_{\text{total}} = J_c + J_{\text{lumped}}$, J_c being the conduction current, and J_{lumped} being the density current due to a given lumped element. In the case of a current source in the y direction, we can derive the following formulation to implement the drain of a transistor inside an FDTD grid. The drain current and its density are given by

$$I_d = g_m \cdot V_{\text{GS}}$$

$$J_d = \frac{g_m \cdot V_{\text{GS}}}{\Delta x \cdot \Delta z}$$

For a parallel resistance and capacitance, we define the two coefficients Coeff1 and Coeff2 as:

$$\text{Coeff1} = 1 - \frac{\Delta t \cdot \Delta y}{2 \cdot \varepsilon_r \cdot R \cdot \Delta x \cdot \Delta y} + \frac{C \cdot \Delta y}{\varepsilon_r \cdot \Delta x \cdot \Delta z}$$

$$\text{Coeff2} = 1 + \frac{\Delta t \cdot \Delta y}{2 \cdot \varepsilon_r \cdot R \cdot \Delta x \cdot \Delta z} + \frac{C \cdot \Delta y}{\varepsilon_r \cdot \Delta x \cdot \Delta z},$$

which leads to the following updated equations:

$$E_y|_{i,j,k}^{n+1} = \frac{\text{Coeff1}}{\text{Coeff2}} * E_y|_{i,j,k}^{n} + \frac{\frac{\Delta t}{\varepsilon_r}}{\text{Coeff2}} * \nabla \times H_y|_{i,j,k}^{n+\frac{1}{2}}.$$

Those coefficients are derived from a semi-implicit scheme used to avoid unstability. When we add the current source, it is straightforward to obtain the following updated equation:

$$E_y|_{i,j,k}^{n+1} = \frac{\text{Coeff1}}{\text{Coeff2}} * E_y|_{i,j,k}^{n} + \frac{\frac{\Delta t}{\varepsilon_r}}{\text{Coeff2}} * \nabla \times H_y|_{i,j,k}^{n+\frac{1}{2}} + \frac{g_m \cdot \Delta t \cdot \Delta y}{\varepsilon_r \cdot \Delta x \cdot \Delta z \cdot \text{Coeff2}} E_y|_{i,j,k-p}^{n},$$

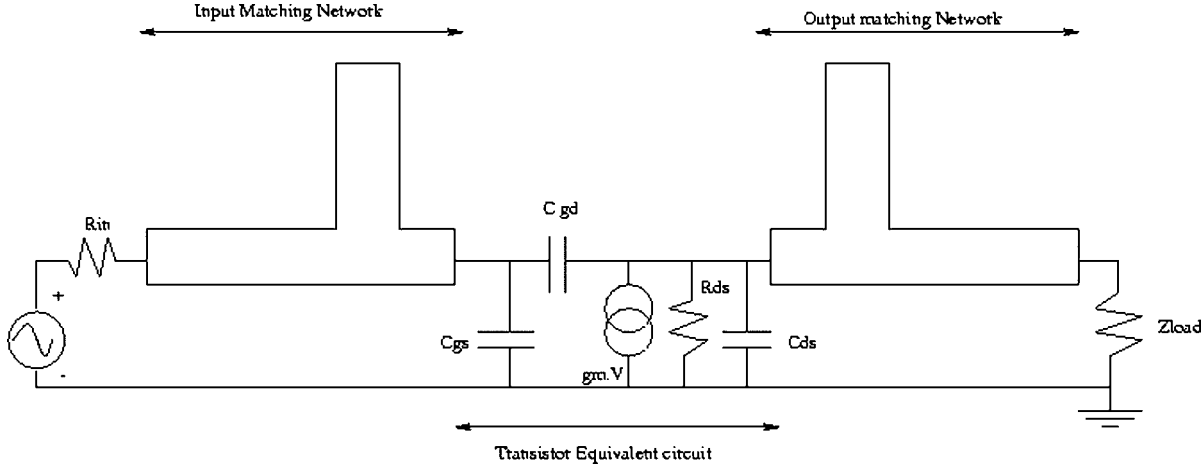

Figure 3. Basic amplifier with matching networks and intrinsic transistor model.

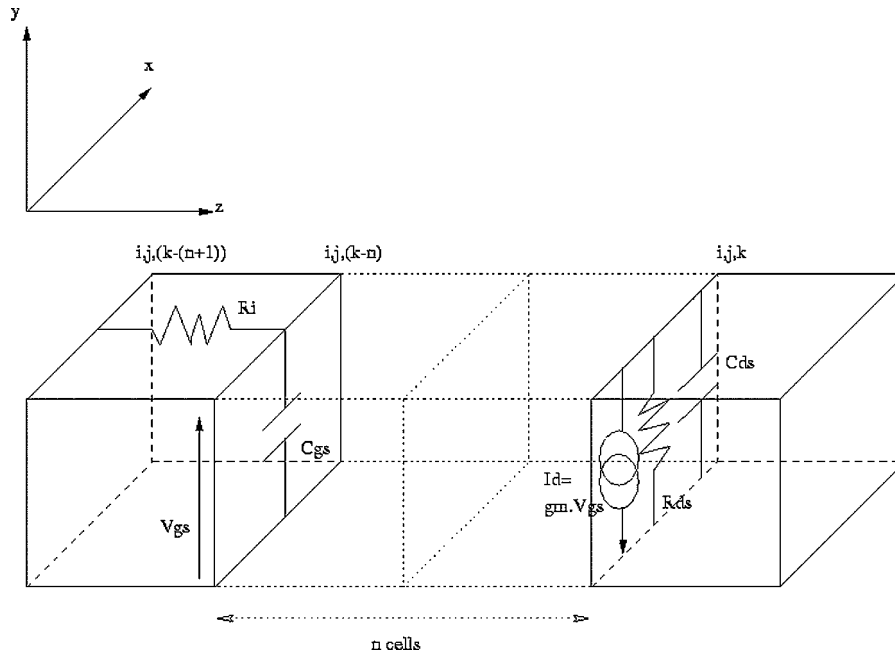

Figure 4. Equivalent circuit parameters of the transistor inserted in the FDTD grid.

where V_{GS} is computed as the integral of the electric field from the ground plane to the strip. In the previous equation, we assumed that the gate and the drain of the transistor were separated by p cells. Thus, the gate voltage is calculated at the $k-p$ cell in the z direction.

The values of R_{ds}, C_{ds}, g_m at the output, and C_{gs} at the input, are updated according to the gate and the drain voltages obtained from the electric field, thanks to the ANN model. This leads to a first-order approximation of the device-wave interaction and to a large-signal analysis.

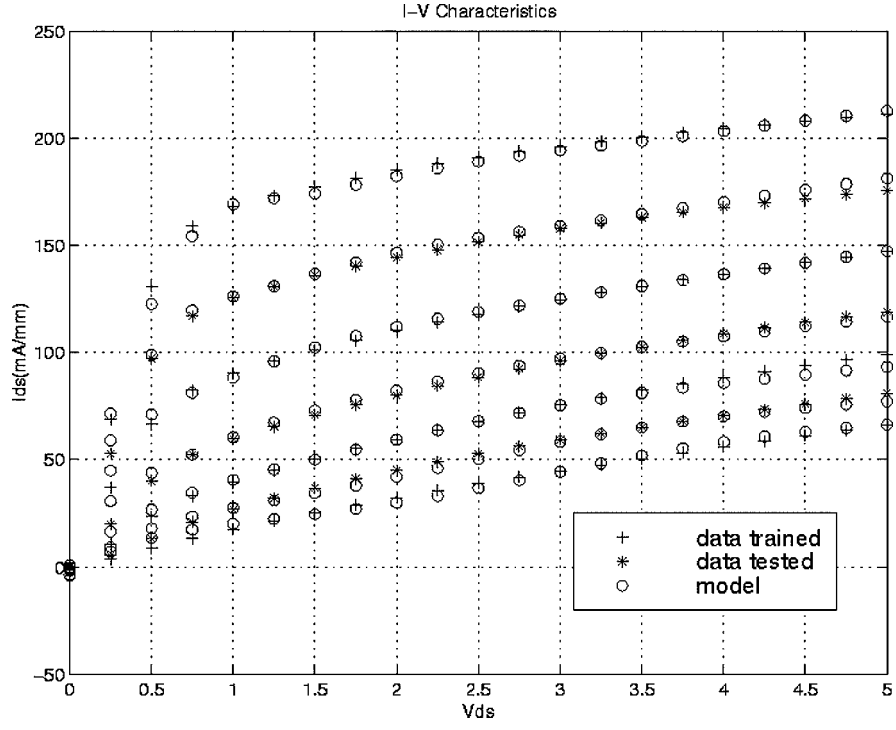

Figure 5. I–V characteristics of the simulated MESFET, hydrodynamic model, and ANN.

V. RESULTS

A typical MESFET was simulated according to the hydrodynamic model presented in section 2. Then a three-layer neural network was trained to model the nonlinearities of Q_{gs}, R_{ds}, Q_{ds}, Q_{gd}, and g_m. Six neurons were used in the hidden layer. Figure 5 shows the I–V characteristics of the simulated MESFET and the results obtained after training of the ANN. The agreement for both sets of data used for training–testing and the hydrodynamic model initial data is very good.

The accuracy is better than 1%. At a given V_{gs}, the drain current can be computed for the whole range of V_{ds} almost instantaneously. This has to be compared with the 45 min. necessary to compute 21 points using the hydrodynamic model on the same computer. Hence, an operating point can be predicted using the ANN without requiring to solve for the hydrodynamic set of equations.

The ANN can be used to calculate the transconductance, g_m. Figure 6 shows the transconductance for three different V_{ds} values. The agreement is very good, which means that the nonlinearities of the MESFET are well modeled using the ANN. Figure 7 shows the gate-to-source charge that leads to the capacitance of the equivalent circuit presented in Figure 8. The neural network predicts very well the nonlinearities of the charges. The same results are obtained for the drain-to-source charges.

We simulated the transistor without any matching network to validate the method. The dielectric constant of the substrate is $\varepsilon_T = 2.2$, and the height of the substrate is $h = 0.794$ mm. The amplifier is assumed to be bias at $V_{GS} = -0.6$ V and $V_{DS} = 3$ V. At this bias point, $C_{gs} = 0.5$ pF, $C_{ds} = 17$ fF, $R_{ds} = 120\,\Omega$, and $g_m = 120$ mS. These results are compared with a simulation performed using HP-Libra, and the trend of S_{21} and S_{11} is close to the FDTD results as shown in Figure 9. Figures 10 and 11 show the time domain results of a small-signal FDTD simulation. The structure is excited by a gaussian pulse(dashed line in Fig. 10). The total input voltage is represented by the solid line, whereas the dashed–dotted lines represent the output total voltage at two different positions in the z-axis. We can observe at the output that the incident wave has been amplified, and that it travels in the $+z$ direction. It is to be noted that the output is perfectly matched with a PML wall. Figure 11 demonstrates the same behavior, but in this case, we have the total output voltage versus z. The structure is divided in 111 cells in the z direction with $dz = 0.4233$ mm. At $t = 0.88$ ps, the incident wave has not reached the transistor yet, but at $t = 1.76$ ps it goes out of the transistor. Then we can notice that the wave is amplified, and also that a discontinuity is observed at $n = 55$, which is the location of the current source. At $t = 2.64$ ps, the wave is out of

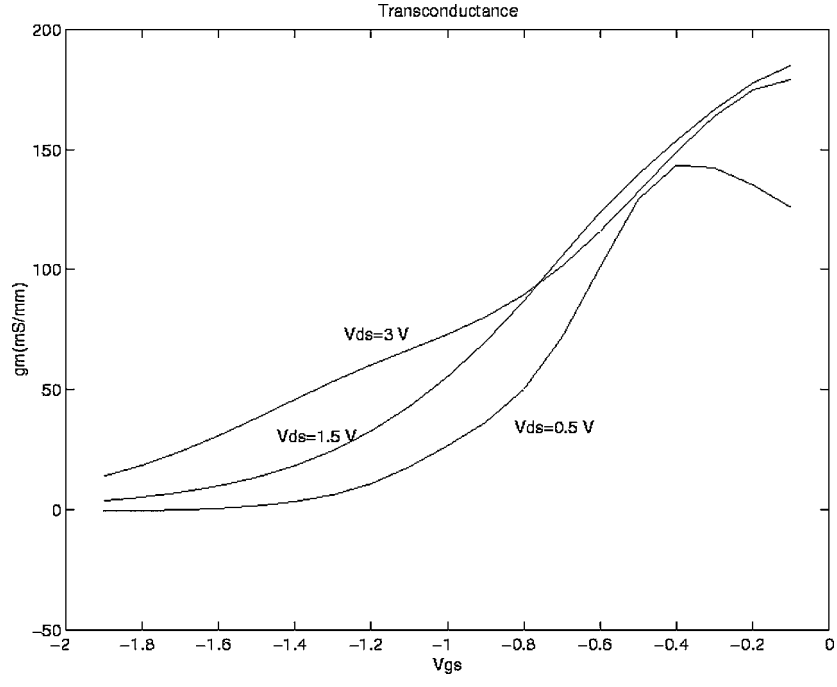

Figure 6. Transconductance computed from the ANN results.

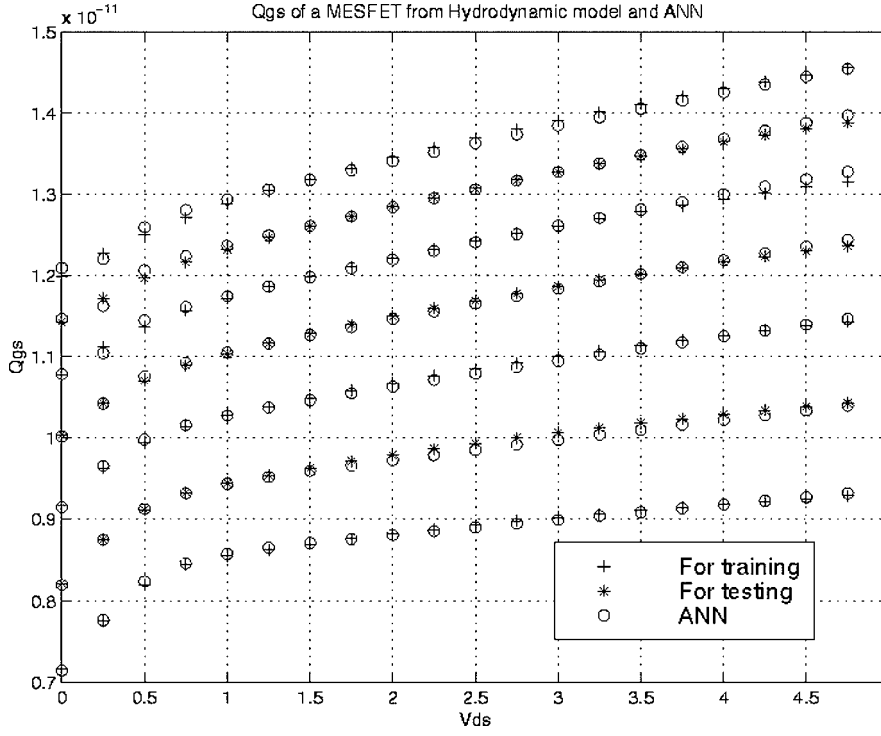

Figure 7. Gate-to-Source charges, Q_{GS}, Hydrodynamic model, and ANN results.

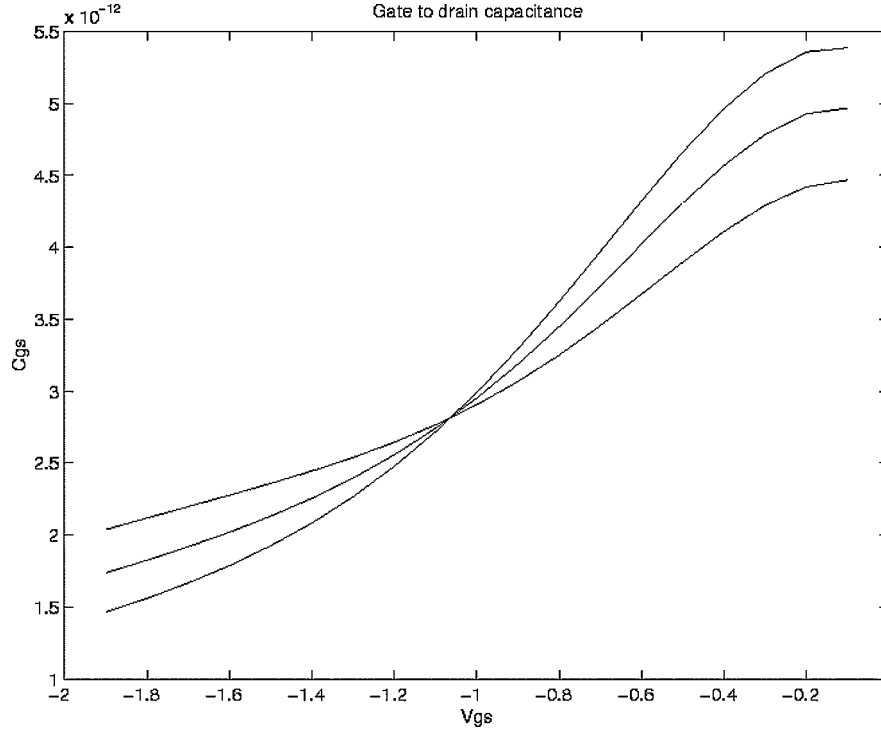

Figure 8. Gate-to-source capacitance, C_{GS} computed from the ANN results.

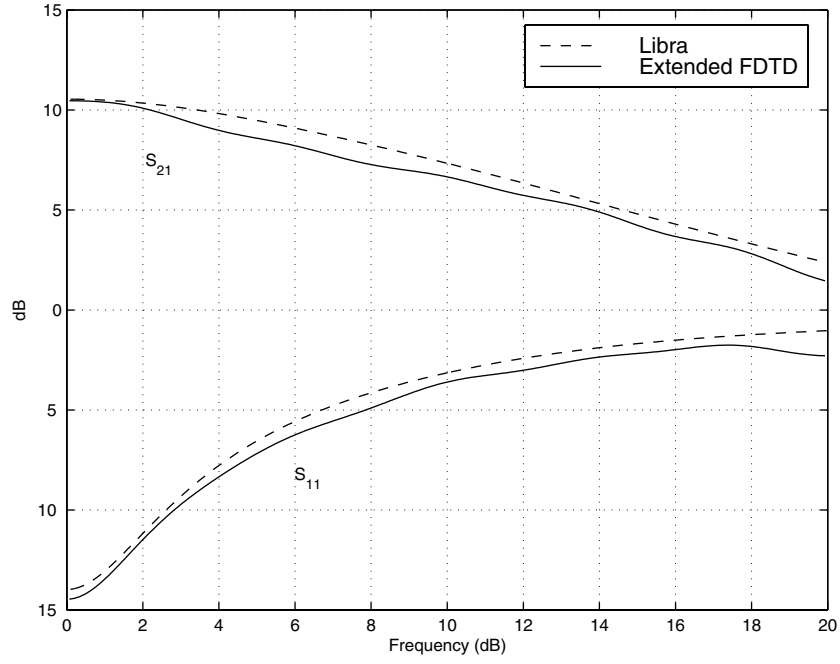

Figure 9. Comparison: The trends of S_{21} and S_{11} using HP-Libra close to the FDTD results.

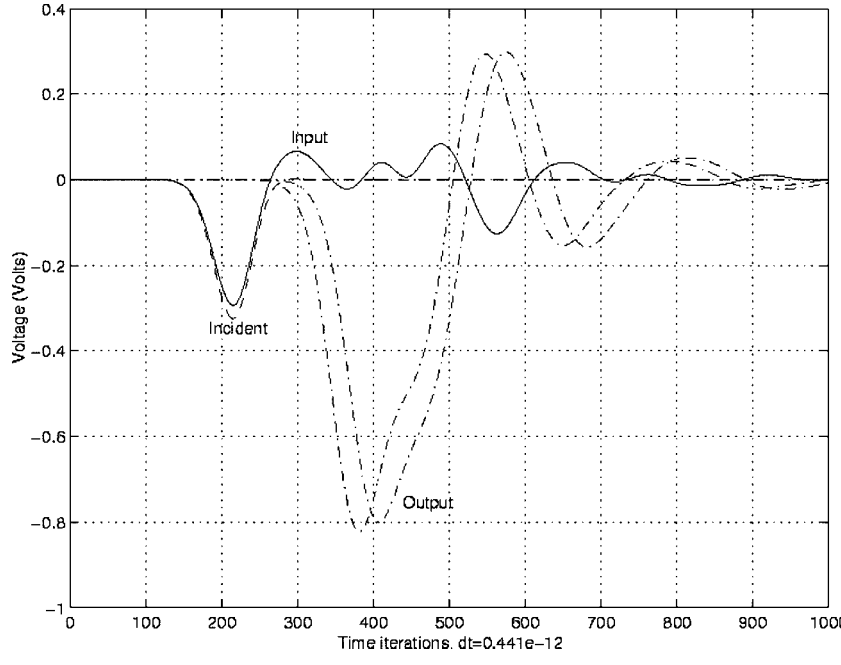

Figure 10. Time domain response of the small-signal amplifier.

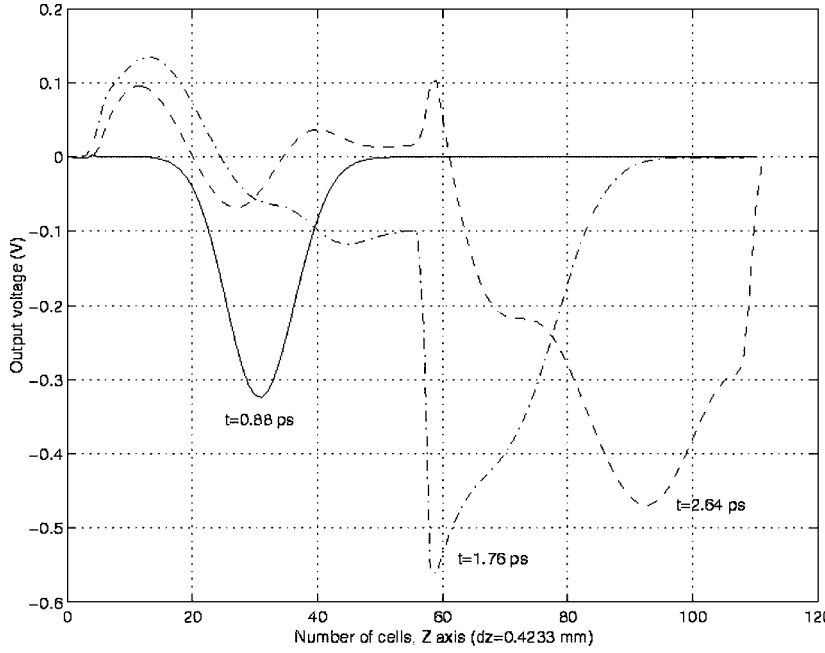

Figure 11. Output voltage versus distance in the z-axis at three different times.

the active region, and it is widely spread over the z-axis. A reflected wave is also observed.

Then the neural network has been used to take into account the nonlinearities of the intrinsic parameters. The structure is excited by a sinusoidal wave of amplitude E_{in} and frequency $f = 10$ GHz. Figure 12 presents the output voltage for three different cases. As the signal gets larger, the wave starts to saturate and generates harmonics in the frequency domain. Figure 13 shows the output voltage in the frequency domain. In each case, the output voltage has been normalized to its maximal value. We can observe that at small signals no harmonics are generated, but as expected second and third harmonics are obtained for the two other cases.

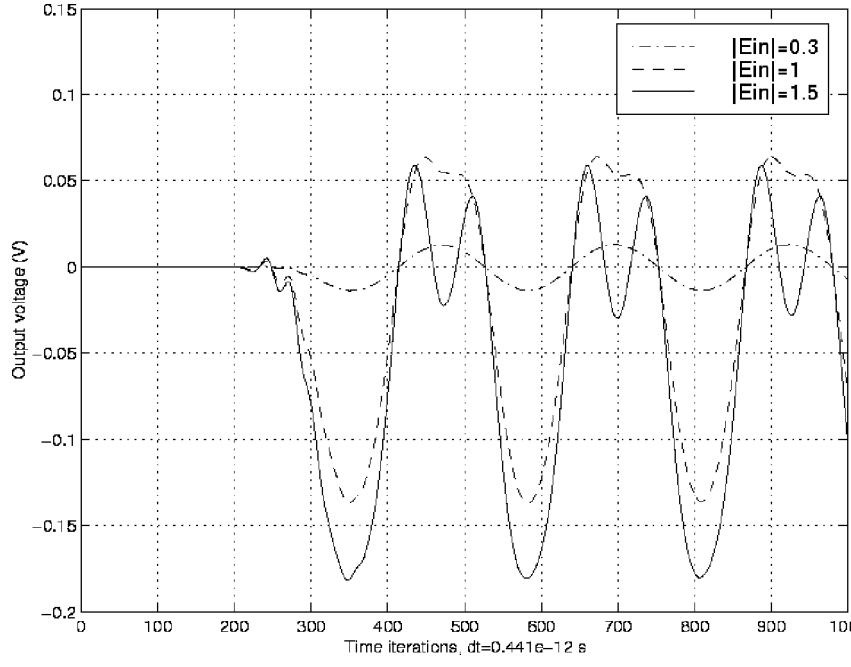

Figure 12. Time domain response of the large-signal simulation.

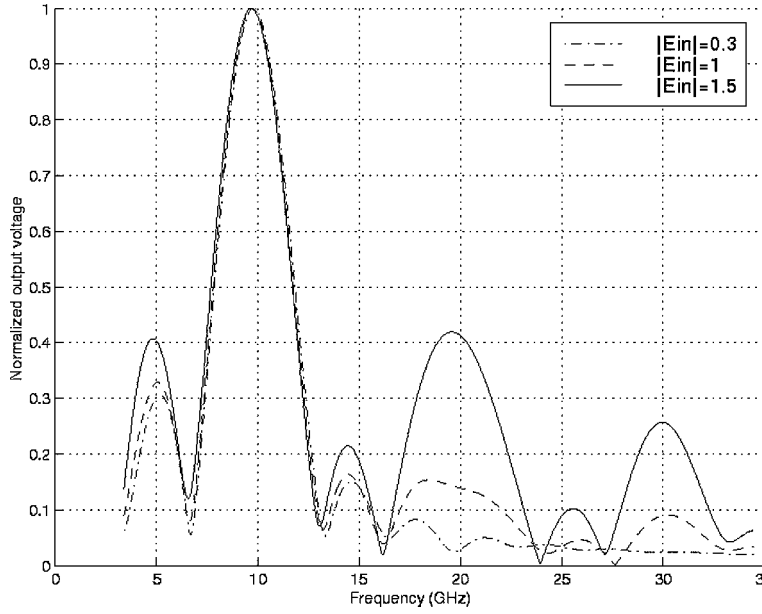

Figure 13. Harmonics obtained from a large-signal simulation using the ANN.

VI. CONCLUSIONS

Millimeter-wave CAD requires a full-wave analysis of MMICs to predict accurately wave-device interactions and the performances of new active devices inside a particular microwave topology. An ANN is used to model the nonlinearities of an MESFET based on a full-hydrodynamic model. This ANN is used to update the intrinsic parameter values of the transistor implemented in the FDTD marching time algorithm as lumped elements. The ANN reduces dramatically the computation time in comparison with a complete global modeling approach. This approach provides an efficient and an accurate first-order global modeling approximation. This is a good candidate for practical millimeter wave CAD.

REFERENCES

1. M.A. Alsunaidi, S.M.S. Imtiaz, and S.M. El-Ghazaly, Electromagnetic wave effects on microwave transistors using a full-wave time-domain model, IEEE Trans Microwave Theory Tech 44 (1996), 799–808.
2. S.M.S. Imtiaz and S.M. El-Ghazaly, Global modeling of millimeter-wave circuits: Electromagnetic simulation of amplifiers, IEEE Trans Microwave Theory Tech 45 (1997), 2208–2216.
3. T.-W. Huang, B. Houshmand, and T. Itoh, The implementation of time-domain diakoptics in the FD-TD method, IEEE Trans Microwave Theory Tech 42 (1994), 2149–2155.
4. K.C. Gupta, Emerging trends in millimeter-wave CAD, IEEE Trans Microwave Theory Tech 46 (1998), 747–755.
5. P.M. Watson and K.C. Gupta, EM-ANN models for microstrip vias and interconnects in dataset circuits, IEEE Trans Microwave Theory Tech 44 (1996), 2495–2503.
6. G.L. Creech et al., Artificial neural networks for fast and accurate EM-CAD of microwave circuits, IEEE Trans Microwave Theory Tech 45 (1997), 794–802.
7. P.M. Watson and K.C. Gupta, Design and optimization of CPW circuits using EM-ANN models for CPW components, IEEE Trans Microwave Theory Tech 45(12) (1997).
8. T.-S. Horng and C.-C. Wang, Microstrip circuit-design using neural-networks, IEEE Microwave Theory Tech Symposium Dig, (1993), 413–416.
9. A. Veluswami, M. Nakhla, and Q.-J. Zhuang, The application of neural networks to EM-based simulation and optimization of interconnects in high speed VLSI circuits, IEEE Trans Microwave Theory Tech 45 (1997), 712–723.
10. A.H. Zaabab, Q.-J. Zhang, and M. Nakhla, A neural network modeling approach to circuit optimization and statistical design, IEEE Trans Microwave Theory Tech 43 (1995), 1349–1358.
11. Shirakawa et al., A large signal characterization of a HEMT using a multilayered neural network, IEEE Trans Microwave Theory Tech 45(9) (1997).

12. C.N. Kuo, B. Housmand, and T. Itoh, Full wave analysis of packaged microwave circuits with active and nonlinear devices: An FDTD approach, IEEE Trans Microwave Theory Tech 45 (1997), 819–826.
13. M. Piket-May, A. Taflove, and J. Baron, FD-TD modeling of digital signal propagation in 3-D circuits with passive and active loads, IEEE Trans Microwave Theory Tech 42 (1994), 1514–1523.
14. W. Sui, D.A. Christensen, and C.H. Durney, Extending the two-dimensional FDTD method to hybrid electromagnetic systems with active and passive lumped elements, IEEE Trans Microwave Theory Tech 40 (1992), 724–730.
15. V.A. Thomas et al. FDTD analysis of an active antenna, IEEE Microwave Guided Wave Lett 4(9) (1994).
16. V.A. Thomas et al. The use of SPICE lumped circuit as sub-grid models for FDTD analysis, IEEE Microwave Guided Wave Lett 4(5) (1994).

BIOGRAPHIES

Sebastien Goasguen was born on March 22, 1974 in Rennes, France. He obtained his Bachelor's degree in Electrical Engineering from the Polytechnic Institute of Toulouse, France in 1997. Then in 1998, he graduated with honors from King's College of London, England with a Master of Science in electronics research. He arrived at Arizona State University in the summer of 1998. He successfully defended his dissertation in August 2001. His area of research is large and ranges from linearization techniques and MMIC design to numerical techniques and semiconductor modeling. In September 2001, he will take a full-time postdoctoral position at Purdue University to work on nanotechnology and molecular electronics.

Samir M. El-Ghazaly received the Ph.D. degree, in Electrical Engineering, in 1988 from the University of Texas at Austin. In August 1988, he joined Arizona State University, where he is now a Professor in the Department of Electrical Engineering. He visited and worked at several universities and research centers including Cairo University; the Centre Hyperfrequences et Semiconducteurs at Université de Lille I in France; University of Ottawa in Canada; the University of Texas at Austin; NASA's Jet Propulsion Lab in Pasadena, California; CST-Motorola, Inc., Tempe, Arizona; *iemn,* Université de Lille, France; and the Swiss Federal Research Institute (ETH). His research interests include RF and Microwave circuits and components; microwave and millimeter-wave semiconductor devices, semiconductor device simulations, ultra-short pulse propagation, microwave-optical interactions; linear and nonlinear modeling of superconductor microwave lines, wave-device interactions, electromagnetics, and numerical techniques applied to monolithic microwave-integrated circuits.

Dr. El-Ghazaly is a Fellow of IEEE, an elected member of Commissions A and D of URSI, a member of Tau Beta Pi, Sigma Xi, and Eta Kappa Nu. He was the secretary and the vice-chairman, and currently is the chairman of Commission A of the US National Committee of URSI. He is a member of the Technical Program Committee for the IEEE International Microwave Symposium since 1991, and on the editorial board of the IEEE Transactions on Microwave Theory and Techniques. He was the chairman of the IEEE-Waves and Devices Group, Phoenix Section. He was the chapter funding coordinator and the chairman of the Chapter Activities Committee of the IEEE MTT Society. He is an elected member of the Administrative Committee (AdCom) of the IEEE Microwave Theory and Techniques Society. He is the Editor-in-Chief for the IEEE Microwave and Wireless Components Letters. He was the general chairman of the IEEE MTT-S 2001 International Microwave Symposium, which was held in Phoenix, Arizona, May 2001.